Article

Misfolding of vWF to Pathologically Disordered Conformations Impacts the Severity of von Willebrand Disease

Alexander Tischer,[1] Pranathi Madde,[1] Laurie Moon-Tasson,[1] and Matthew Auton[1,*]
[1]Division of Hematology, Department of Internal Medicine, Mayo Clinic, Rochester, Minnesota

ABSTRACT The primary hemostatic von Willebrand factor (vWF) functions to sequester platelets from rheological blood flow and mediates their adhesion to damaged subendothelium at sites of vascular injury. We have surveyed the effect of 16 disease-causing mutations identified in patients diagnosed with the bleeding diathesis disorder, von Willebrand disease (vWD), on the structure and rheology of vWF A1 domain adhesiveness to the platelet GPIbα receptor. These mutations have a dynamic phenotypical range of bleeding from lack of platelet adhesion to severe thrombocytopenia. Using new rheological tools in combination with classical thermodynamic, biophysical, and spectroscopic metrics, we establish a high propensity of the A1 domain to misfold to pathological molten globule conformations that differentially alter the strength of platelet adhesion under shear flow. Rheodynamic analysis establishes a quantitative rank order between shear-rate-dependent platelet-translocation pause times that linearly correlate with clinically reported measures of patient platelet counts and the severity of thrombocytopenia. These results suggest that specific secondary structure elements remaining in these pathological conformations of the A1 domain regulate GPIbα binding and the strength of vWF-platelet interactions, which affects the vWD functional phenotype and the severity of thrombocytopenia.

INTRODUCTION

"Diathesis" refers to the tendency to suffer from a medical condition, particularly a "hereditary or fundamental predisposition to a state or condition of disease or a disorder involving structural or metabolic abnormalities." von Willebrand disease (vWD) constitutes a very common bleeding diathesis with an estimated epidemiological prevalence of ~1% of the human population (1). Over the course of the last few decades, clinical diagnostics have enabled the classification of this disorder into three distinct types (vWD types 1–3) of von Willebrand factor (vWF) deficiency. vWF, a multimeric glycoprotein secreted from the vascular endothelium, mediates platelet adhesion to exposed subendothelial connective tissue and contributes to the arrest of bleeding during primary hemostasis. It consists of multiple copies of A, B, C, and D domains that are arranged in the order D′-D3-A1-A2-A3-D4-B1-B2-B3-C1-C2-(cysteine knot).

Type-1 and type-3 vWD results in partial or complete quantitative deficiencies of vWF from blood plasma. The qualitative functional deficiencies of vWF associated with type-2 vWD result in one of the following: defective interactions between the A1 domain and the GPIbα platelet receptor, loss of hemostatic activity due to abnormal multimer proteolysis of the A2 domain by the ADAMTS-13 plasma protease, or deficient binding of the D domains to FVIII.

Type-1 vWD accounts for ~65–80% of cases; type-2 vWD, ~20–35%; and type-3 is extremely rare (2). Of 399 unique mutations identified in the vWF gene associated with vWD, 160 are associated with type-2 vWD and 54 of these directly affect binding between A1 and GPIbα (3) in the vWD subtypes 2B and 2M. These subtypes categorically represent either an increased (2B) or reduced/deficient (2M) vWF-dependent platelet adhesion. Missense mutations in these vWD subtypes have a dynamic range of clinical manifestations from a paucity of vWF-platelet interactions to severe thrombocytopenia resulting in bleeding at both extremes of vWF dysfunction.

From the time of early observations of impaired platelet adhesion to the subendothelium in vWD (4) and following the isolation and characterization of the vWF gene, protein, and domain structure (5–7), the general perception has been that mutations affecting the adhesion of platelets to vWF alter the conformation of the A1 domain. This idea has been prevalent even in the early literature describing the patients afflicted by the specific missense amino-acid substitutions causing the disease. Type 2B mutations were presumed to alter the conformation of vWF multimers and increase exposure of the GPIb binding site (8) such that vWF could mimic the effect of subendothelial matrix or collagen binding, causing pathologic spontaneous platelet aggregation (SPA) (9).

Conversely, a complete loss-of-function, type 2M mutation was thought to inhibit the normal allosteric regulation of GPIb binding (10). The concept of allosterism took precedence as more mutations were identified and the regulation of vWF interaction with platelet GPIb was thought to involve an equilibrium between binding-competent and

Submitted January 31, 2014, and accepted for publication July 9, 2014.
*Correspondence: auton.matthew@mayo.edu
Editor: Josh Wand.

0006-3495/14/09/1185/11 $2.00
http://dx.doi.org/10.1016/j.bpj.2014.07.026

incompetent states. More recently, it has been suggested that type 2M mutations could destabilize the global fold of the A1 domain resulting in loss of function (11–13). The first evidence of distinctly different GPIb binding conformations in the recombinant A1 domain was observed when reduction and alkylation of the disulfide bond enhanced GPIb binding affinity and reversed the shear flow dependency of platelet adhesion (14,15).

Our initial studies took a thermodynamic perspective when we directly observed a stable, partially unfolded intermediate conformation of the A1 domain in the denaturant unfolding pathway (16). To model this intermediate, we reduced-and-carboxyamidated (RCAM) the A1 domain and found increased affinity for platelet GPIb. Combined with unfolding studies of A1 harboring a few mutations, we developed a thermodynamic cycle that described the A1-GPIb interaction in terms of an equilibrium between low- and high-affinity conformations. This model was consistent with previous concepts of allosterism while bringing protein folding to the forefront of the issue, but it did not account for situations in which the A1 domain could misfold to inactive conformations (17,18). Recently we have demonstrated that RCAM A1 exists in a molten globule state, a conformation lacking global tertiary structure while retaining secondary and potential supersecondary structure elements. These structural elements in RCAM A1 are sufficient to maintain high affinity for GPIb such that platelets remain firmly attached under shear flow (19).

Here, we illustrate that the predisposition of the platelet GPIbα binding A1 domain of vWF is toward a partially disordered molten globule state involving mutation-induced structural abnormalities that specifically alter the shear-dependent function of vWF. We have recombinantly engineered 16 of the most commonly reported type 2B and 2M mutations into the A1 domain of vWF and compared their effect on shear-dependent platelet adhesion and the conformational and thermodynamic properties of A1. All proteins excepting five type 2M variants of the A1 domain supported shear-flow-dependent platelet adhesion to surface-captured A1 domain variants in a parallel plate flow-chamber. We have analyzed the strength of platelet adhesion by taking the statistical average of pause-time distributions, a measure of the average time platelets remain immobile under shear flow. These pause times are significantly correlated to reported vWD patient platelet counts (R^2 = 0.88) and the severity of thrombocytopenia indicating the structural and functional properties of the isolated A1 domain variants are representative of plasma vWF platelet interactions.

Using established conformational metrics (19), only six of the 18 variants (including WT and RCAM A1) are natively structured, and 10 of the remaining 12 variants are molten globules. One type 2M mutation reduced platelet adhesion relative to WT, five type 2M mutations resulted in molten globules with a complete loss of function, and four type 2B mutations induced molten globule states that differentially enhance platelet pause times under rheological shear flow. The structural locations of these mutations in the A1 domain (Fig. 1) suggest that allosteric effects in addition to localized effects of mutations on the α2-helix loop α3-helix may regulate the adhesive strength of the A1-GPIbα tether bond. Our results provide the first experimental evidence, to our knowledge, of A1 domain misfolding to disordered conformations and indicate that the pathobiological function of the vWF A1 domain depends on secondary structure elements remaining in these disordered states.

MATERIALS AND METHODS

Mutagenesis, expression, purification, and quantification treatments of the vWF A1 variants are described in the Supporting Material.

Biophysical, structural, and thermodynamic metrics

Circular dichroism measurements were performed on a model No. 420C circular-dichroism spectrometer (Aviv Biomedical, Lakewood Township, NJ). All fluorescence (FL) measurements were performed on a Fluorolog 3 spectrofluorometer (HORIBA Jobin-Yvon, Edison, NJ) equipped with a model No. LF1-3751 temperature controller (Wavelength Electronics, Bozeman, MT). Near- and far-ultraviolet (UV) circular dichroism (CD), intrinsic protein FL, and ANS (8-anilino naphthalene sulfonic acid) CD spectra were determined as described in Tischer et al. (19). Urea

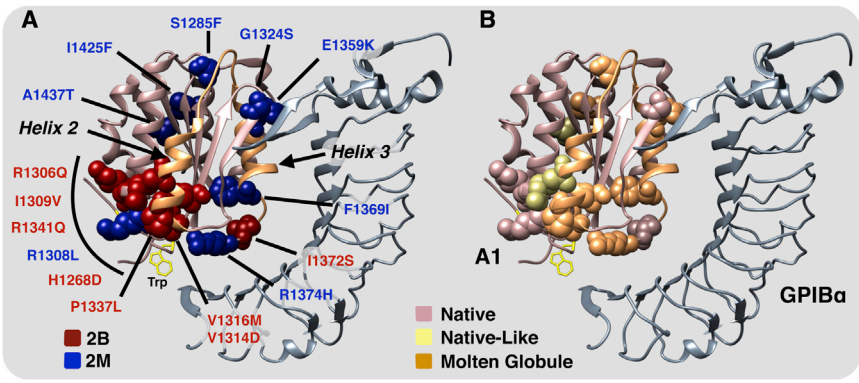

FIGURE 1 Structure of the A1 domain in complex with GPIbα with locations of type 2B (*red*) and 2M (*blue*) vWD mutations (*A*) and colored by conformational class (*B*); native (same color as A1 structure), nativelike (*yellow*), and molten globule (*orange*). (Helices 2 and 3 are also indicated in *orange*.) The tryptophan residue is indicated for reference to FL studies. PDB:1SQ0. See Movie S1 in the Supporting Material. We used CHIMERA, Ver. 8.6.1 (https://www.cgl.ucsf.edu/chimera/). To see this figure in color, go online.

denaturation (monitored by far-UV CD) and thermal denaturation (monitored by far-UV CD, intrinsic protein FL, and ANS FL) were performed and analyzed as previously described (19,20). Acrylamide quenching of intrinsic tryptophan fluorescence was performed and analyzed as described in Tischer et al. (19). All spectra were collected at 20°C.

Parallel plate flow-chamber studies

The rheological interaction of platelets with A1 domain variants harboring type 2M and type 2B mutations was studied using recently developed flow-chamber methods (19). The A1 domains (5 μM) were immobilized on Vena8 biochips (Cellix, Dublin, Ireland) coated with a Cu^{2+}-chelated polyethylene-glycol surface serviced by MicroSurfaces, Inc. (Englewood, NJ) via the 6×His-Tag, enabling the preservation of the structural properties of the domain in solution and its concomitant effects on platelet adhesion under rheological shear flow. One-hundred microliters of citrated whole blood, obtained from the informed consent of normal healthy volunteer donors with approval from the Mayo Clinic Institutional Review Board (Rochester, MN), was perfused at a shear rate of 800 s^{-1} followed by Tris-buffered saline. Platelets translocating on the surface-captured domains were filmed at 24 frames/s for 1 min at logarithmic intervals of the shear rate. Coordinates obtained from tracking analysis of the resulting movies were processed using our recently developed statistical analytics for the quantification of cellular adhesion dynamics across immobilized receptors under rheological shear flow (19). Biochips lacking the surface-captured A1 domain were completely inert to platelets.

RESULTS

Thermodynamic and conformational characterization of types 2M and 2B vWF A1 domain variants

We began these studies by assessing the effects of mutations on the thermodynamic stability of A1 (18) and developed a framework that incorporated partial unfolding as a means for enhancing the binding affinity of A1 for GPIbα (17). Initially, we used the urea-temperature phase diagram method for assessing the reversible thermodynamics of unfolding at various temperatures (18,21), and more recently we have incorporated thermal denaturations to assess kinetic irreversibility (20,22). We have employed these methods using a variety of spectroscopic observables that assess the conformation of these A1 domain variants as a function of temperature and urea.

These observables include the following:

1. Far-UV CD to assess secondary structure content,
2. Near-UV CD to assess tertiary structure content,
3. Intrinsic protein FL to assess solvent exposure of tyrosine and tryptophan residues,
4. Acrylamide quenching of tryptophan FL to assess local solvent exposure of the single tryptophan residue, and
5. Binding of the molten globule indicator-dye, ANS, to assess exposure of hydrophobic surface area.

In total, these studies have provided metrics that are able to classify the conformation of A1 into three types, based on biophysical spectroscopy, as follows:

Natively structured

In this class, the A1 domain is in its global native fold, but mutations induce local conformations in the native state ensemble that alter its thermodynamic stability against partial unfolding toward an intermediate conformation. The type 2B mutations R1306Q and I1309V and the type 2M mutation G1324S have previously been characterized in this conformational class (18). In addition, R1308L and I1372S also belong to this class.

Nativelike

In this class, the A1 domain has reduced secondary structure content, but retains some of the tertiary structure required for a cooperative urea- or temperature-induced protein unfolding transition. The type 2M mutation A1437T and the type 2B mutation R1341Q belong to this class.

Molten globule

In this class, the A1 domain has a significantly reduced tertiary structure content as defined by the absence of a cooperative urea- or temperature-induced protein unfolding transition and retains only secondary and/or supersecondary structure. The type 2M mutations F1369I, E1359K, I1425F, S1285F, and R1374H, and the type 2B mutations H1268D, P1337L, V1316M, and V1314D, belong to this class.

Fig. 2 and Fig. S1, Fig. S2, Fig. S3, and Fig. S4 in the Supporting Material illustrate urea and thermal denaturations of type 2M and type 2B mutations from each conformational class monitored by Far-UV CD, intrinsic protein FL, and ANS FL for all A1-domain variants studied.

Thermodynamic analysis (see Table S1 in the Supporting Material) of the native variants generally demonstrates that the stability is decreased relative to WT A1 for type 2B gain-of-function variants and the stability is increased for loss of function variants. This is also evident in the unfolding transition midpoints, T^* and $c_{1/2}$, which are lower for gain-of-function and higher for loss-of-function variants. The T^* and $c_{1/2}$ values are also positively correlated so

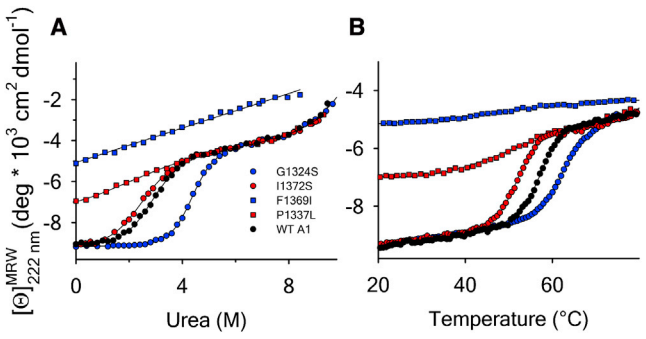

FIGURE 2 Urea denaturation (*A*) and thermal denaturation (*B*) of the A1 domain monitored by CD at 222 nm for the representative variants indicated. (*Red*) Gain-of-function, type-2B. (*Blue*) Loss-of-function, type-2M. To see this figure in color, go online.

that a change in thermal stability is paralleled by a comparable change in urea stability (see Fig. S5). These results remain in general agreement with our previous conclusions (17,18). The nativelike variants, A1437T and R1341Q, also have low stability, but because they are less structured, some regions of the A1 domain are likely to be partially unfolded. Intrinsic protein FL is generally not sensitive to conformational differences between natively structured and nativelike conformations because the FL intensities are similar in both pre- and postthermal unfolding transitions. However, ANS FL does discriminate between these conformations, because the mutations result in exposure of new hydrophobic groups in the A1 domain.

Far-UV and near-UV CD spectra demonstrate reduced secondary structure and a significantly diminished tertiary structure content in molten globules (see Fig. S6). These conformations show an ellipticity in the far-UV that gradually increases with urea and temperature without a sigmoid transition. The type-2M variants, E1359K and F1369I, are the most disordered having ellipticities that are greater than all other variants over the full range of urea and temperature. All other molten globule states have conformations with similar secondary structure content as the urea and thermally unfolded WT A1 domain. P1337L and H1268D are the most structured molten globules. We consider these as borderline with the nativelike class because, although they do not have a urea-induced unfolding transition, thermal denaturation shows a hint of a sigmoid transition at around 50°C by CD, suggesting a slightly more organized cluster of supersecondary structure under native conditions. Intrinsic protein FL intensity of the molten globule variants is higher than native and nativelike variants in the low temperature range, indicating that tyrosine and tryptophan residues are maximally exposed. Likewise, ANS FL intensities of the molten globule class are greater than those for the native and nativelike variants, indicating a greater exposure of hydrophobic groups in the domain.

The spectroscopic metrics used to assess the conformational properties of the A1 domain variants are summarized in Fig. 3, and are also given as follows:

1. The far-UV ellipticity at 222 nm is used as a metric for global α-helical secondary structure content in all domain variants (Fig. 3, *A* and *B*).
2. The Stern-Volmer constant of collisional acrylamide quenching of tryptophan fluorescence is a measure of tryptophan solvent exposure within the local tertiary structure of all domain variants (Fig. 3, *C* and *D*). The greater the magnitude of this constant, the more solvent-exposed the tryptophan, and the greater its susceptibility to fluorescence quenching (see Fig. S7).
3. After thermal denaturation, the A1 domain becomes irreversibly trapped in the molten globule conformation (20), which binds ANS with greater affinity than folded conformations of A1. The ratio of maximal ANS FL intensity at ~475 nm before and after thermal denaturation is used as a metric for the degree of hydrophobicity of the domain relative to that in the postthermal molten globule state (Fig. 3, *E* and *F*). A ratio close to 1 indicates that the domain variant exists as a molten globule in its natural conformation.

Fig. 3 illustrates that these A1 domain variants each have a particular conformational character with respect to these metrics. Ellipticity distinguishes the domain variants as either having native or nonnative secondary structure content. With respect to the tertiary environment of the tryptophan, all molten globules have quenching constants in the range of 4–5/*M*; RCAM A1 is ~6/*M* due to the absence of a disulfide bond. The native and nativelike classes have a greater variability in the quenching constant, and, depending on the location, the mutation could either directly or allosterically affect tryptophan exposure by destabilizing the local region. Similarly, there is much more variability in the ANS intensity ratio in the native and nativelike class depending on localized exposure of the hydrophobic groups induced by the mutations. In general, these metrics are highly correlated with each other among all domain variants (Fig. 4), indicating that losses of secondary and tertiary structure are mutually consequential.

Shear-flow-dependent platelet adhesion to types 2M and 2B vWF A1 domain variants

The pause (residence) time for which a platelet remains immobile is a fundamental parameter obtained from our analysis of the shear-dependent platelet translocations, and is directly proportional to the strength and number of A1-GPIbα bonds. The shear-rate dependency of this parameter correlates with the force-dependent lifetimes of single A1-GPIbα bonds (17,20, 23–25). Fig. 5 shows the statistical mean $\pm$ standard deviation of the shear-rate-dependent pause times. Fig. 5 *A* illustrates representative pause times obtained as a function of shear rate for a type 2B (P1337L) and a type 2M (A1437T) mutation relative to WT A1. Shear-dependent pause times were determined for all A1 variants capable of binding platelets (Fig. 5, *C–E*) categorized according to their experimentally determined conformational classification. In Fig. 5 *B*, the platelet pause times obtained for all variants at the physiological shear rate of 1500 s^{-1} are ranked from least to greatest, ranging from ~0.3 to 3.5 s (see also Table 1). Of the type 2M mutations studied, F1369I, E1359K, I1425F, R1374H, and G1324S did not bind platelets. All type 2B mutations, with the exception of R1308L, bind tighter than the WT A1 domain, resulting in higher pause times at all shear rates. These data demonstrate that the absolute magnitude of the pause time varies considerably with the particular mutation.

We have compiled platelet counts obtained from routine complete blood counts and ristocetin cofactor-dependent

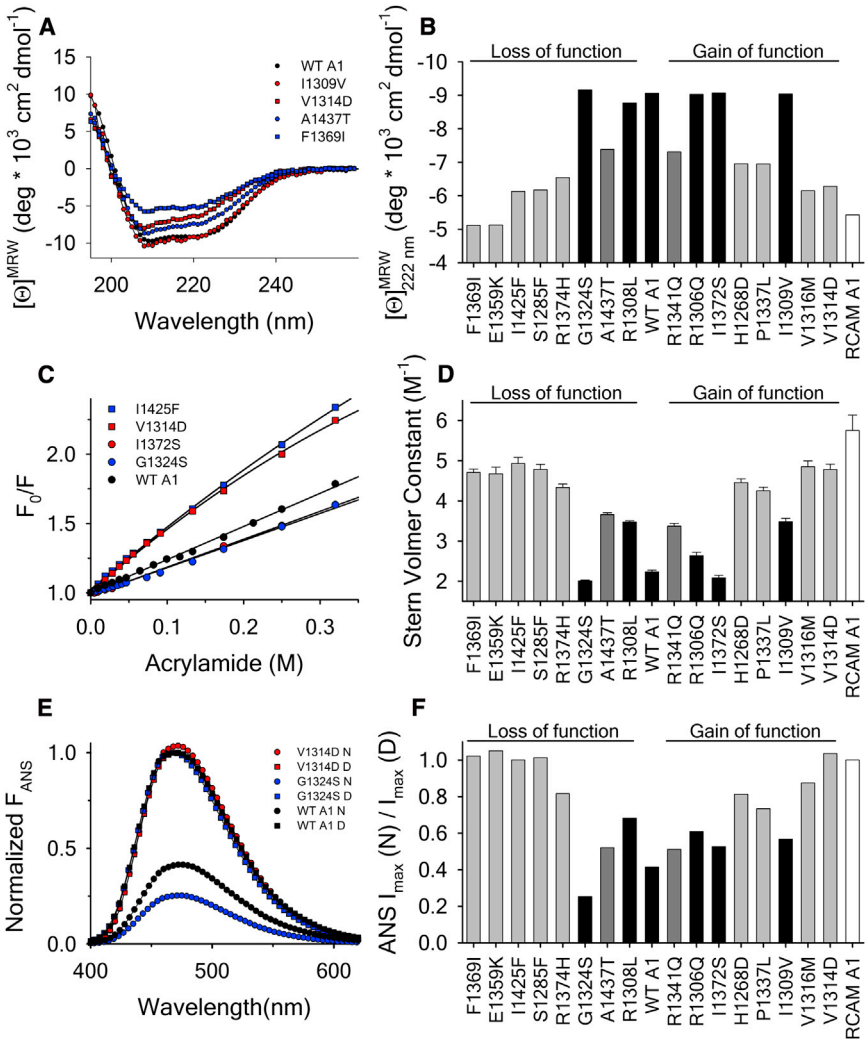

FIGURE 3 Biophysical metrics for secondary and tertiary structure. (*A*) Far-UV CD spectra. (*B*) CD ellipticity at 222 nm. (*C*) Stern-Volmer plots. (*D*) Stern-Volmer collisional quenching constants. (*E*) Normalized ANS FL spectra of native and thermally denatured A1 domain variants. (*F*) ANS intensity ratios. (*Red*) Type 2B and (*blue*) type 2M in panels *A*, *C*, and *E*. (*B*, *D*, and *F*) All variants are ranked according to increasing pause time as in Fig. 5. (*Black*) Natively structured variants. (*Dark gray*) Nativelike variants. (*Light gray*) Molten globule variants. (*White*) RCAM A1. To see this figure in color, go online.

vWF activity relative to vWF antigen (vWF:RCo/vWF:Ag) ratios from clinical case reports (see Table S2), summarized in Table 1 with vWF multimer analysis and unique symptoms. Platelet counts are reported at baseline before any stress-inducing condition, such as pregnancy or desmopressin administration, when such conditions were reported. Type 2M patients typically have below-normal vWF:RCo/vWF:Ag ratios, normal platelet counts (150–400 $\times$ $10^3\mu L^{-1}$), normal

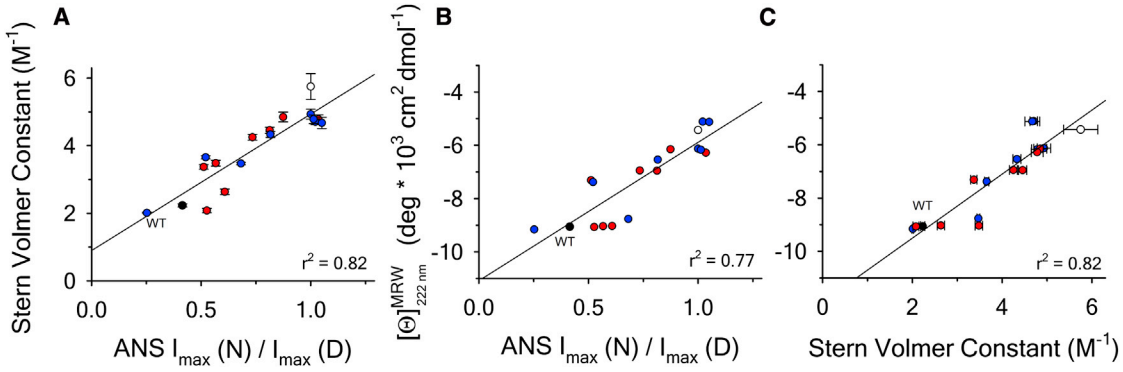

FIGURE 4 Correlation between biophysical metrics for secondary and tertiary structure. (*A*) Stern-Volmer constants versus ANS intensity ratios (R^2 = 0.82). (*B* and *C*) Ellipticity versus ANS intensity ratios (R^2 = 0.77) and Stern-Volmer constants (R^2 = 0.82). (*Red*) 2B; (*blue*) 2M; (*white*) RCAM A1. To see this figure in color, go online.

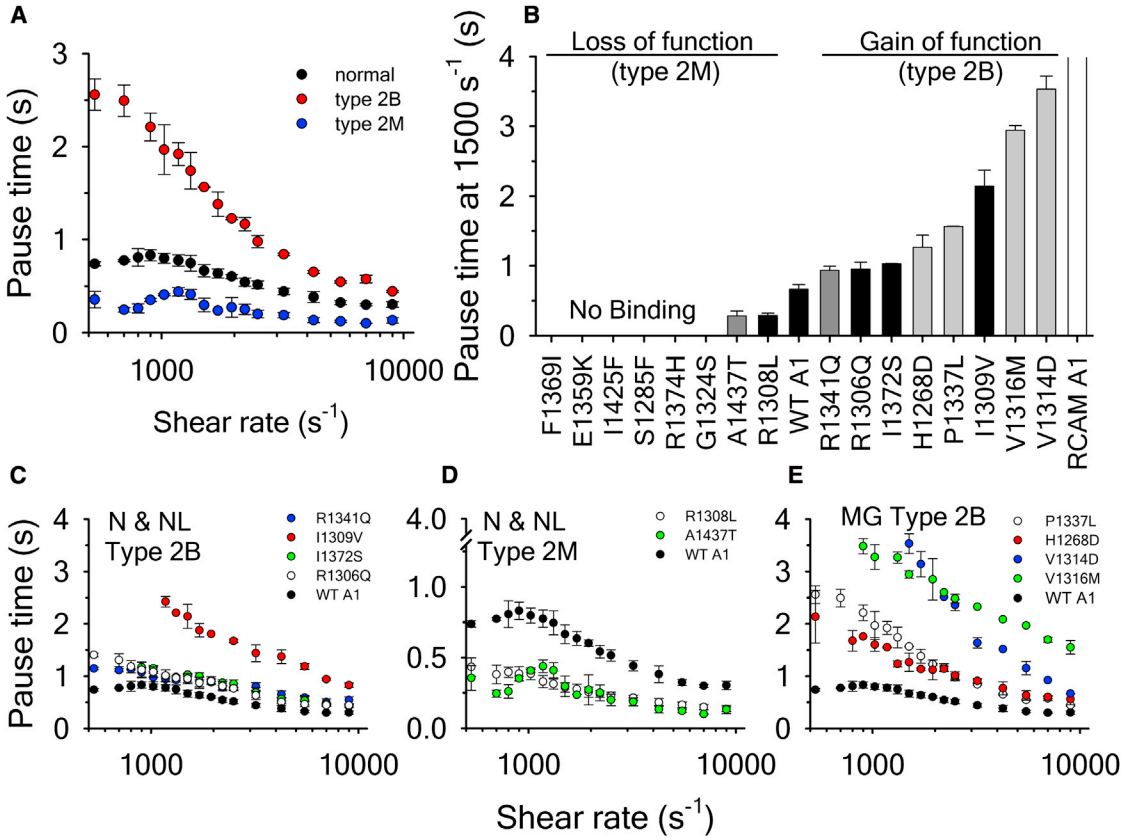

FIGURE 5 (*A*) Shear-rate dependency of platelet pause times on normal (WT A1), type 2B (P1337L), and type 2M (A1437T) variants. (*B*) Rank order of pause times at 1500 s^{-1} shear rate from least to greatest. The type 2M variants F1369I, E1359K, I1425F, S1285F, and R1374H did not bind platelets at any shear rate. (*Solid*) Natively structured variants. (*Dark shaded*) Nativelike variants. (*Light shaded*) Molten globule variants. (*Open*) RCAM A1 represents a case of firm adhesion with no platelet translocation due to loss of the disulfide bond (19). Shear-rate dependency of platelet pause times on (*C*) natively structured type 2B A1 domain variants, (*D*) natively structured type 2M A1 domain variants, and (*E*) molten globule A1 domain variants. To see this figure in color, go online.

vWF multimerization, decreased or absent ristocetin-induced platelet binding (RiPB), and either normal or decreased platelet binding induced by the snake venom botrocetin (BiPB). Type 2B patients typically have normal to diminished vWF:RCo/vWF:Ag ratios, vWF multimers lacking high-molecular-weight (HMW) species, platelet counts ranging from normal to severely thrombocytopenic, and in some cases, spontaneous platelet aggregation, which occurs in the absence of shear stress.

In Fig. 6, the mean ± standard deviation of all reported platelet counts and vWF:RCo /vWF:Ag ratios are plotted as a function of our experimentally determined mean ± standard deviation platelet pause times at 1500 s^{-1}. Although many of the platelet counts are within the normal range, Fig. 6 *A* demonstrates a linear correlation with a coefficient of determination $R^2 = 0.88$. Mutations with the highest pause times (I1309V, V1316M, and V1314D) vary from moderate to severe thrombocytopenia. This high level of correlation demonstrates that the pause times determined from our experimental system are of diagnostic quality in that they trend with thrombocytopenic severity. This trend indicates that the functional and conformational properties of the single A1 domain are representative of the intrinsic properties governing the interaction between platelet GPIb and multimeric vWF in vivo. Conversely, vWF:RCo/vWF:Ag ratios are not correlative to experimental pause times (Fig. 6 *B*), and there is no correlation between vWF:RCo/vWF:Ag and platelet count ($R^2 = 0.06$).

DISCUSSION

A considerable challenge for accurate diagnoses of qualitative vWD subtypes remains prominent. Although the rare type-3 quantitative deficiency can be identified by the virtual absence of plasma vWF using vWF:Ag tests, the more common type-1 quantitative and type-2 qualitative deficiencies are more prone to subtype misdiagnosis due to disconcordance of vWF:RCo activity relative to vWF:Ag (28). Thrombocytopenia is a strong indicator of type 2B, but it need not be present for mild variants. Distinguishing type 2M is usually dependent on the absence of ristocetin-induced platelet agglutination (RIPA) and a

TABLE 1 Structure/Function properties of type-2 vWD variants of the A1 domain and their clinical manifestations in vWD patients

Mutation (vWD type)[a]	A1 domain conformation[b]	Pause time 1500 s^{-1} (s)[c]	vWF:RCo/vWF:Ag[d]	Patient platelet count ($\times 10^3/\mu L$)[d]	Patient vWF multimers[e]	Unique symptoms[f]
F1369I (2M)	MG	NB (2)	0.34 ± 0.19 (4)	NR	Normal	↓ RiPB, normal BiPB
E1359K (2M)	MG	NB (2)	0.55 (1)	NR	NR	↓ RiPB, normal BiPB
I1425F (2M)	MG	NB (2)	0.34 ± 0.2 (4)	NR	Normal	↓ RiPB, normal BiPB
S1285F (2M)	MG	NB (2)	0.39 ± 0.05 (3)	348 ± 55 (3)	↓ HMW	↓ RiPB, ↓ BiPB
R1374H (2M)	MG	NB (2)	0.36 ± 0.18 (50)	239 ± 56 (6)	↓ HMW with ATS	↓ RiPB, ↓ BiPB
G1324S (2M)[g]	N	NB (3)	0.31 ± 0.13 (4)	278 ± 47 (3)	Normal	Absent RiPB, normal BiPB
A1437T (2M)	NL	0.28 ± 0.07 (3)	0.47 ± 0.04 (4)	NR	NR	Mild moderate bleeding
R1308L (2B)	N	0.29 ± 0.03 (5)	0.88 ± 0.17 (16)	298 ± 85 (11)	Normal	↓ Collagen binding
WT A1	**N**	**0.67 ± 0.07** (6)	**0.7–1.2**	**150–400**	**Normal**	**Normal**
R1341Q (2B)	NL	0.94 ± 0.06 (5)	0.56 ± 0.18 (27)	188 ± 85 (23)	Absent HMW	Moderate bleeding with TCP
R1306Q (2B)	N	0.95 ± 0.1 (3)	0.73 ± 0.14 (5)	219 ± 36 (5)	Normal	Mild TCP
I1372S (2B)	N	1.03 ± 0.004 (2)	0.82 ± 0.13 (2)	256 ± 33 (2)	Normal	SPA
H1268D (2B)	MG	1.26 ± 0.17 (4)	0.61 ± 0.21 (5)	208 ± 79 (8)	↓ HMW	Intermittent mild TCP
P1337L (2B)	MG	1.56 ± 0.005 (4)	0.84 ± 0.22 (10)	165 ± 84 (7)	↓ HMW	Moderate TCP
I1309V (2B)	N	2.14 ± 0.23 (3)	0.72 ± 0.09 (14)	109 ± 11 (13)	Normal	SPA and persistent moderate TCP
V1316M (2B)	MG	2.94 ± 0.07 (4)	0.45 ± 0.25 (47)	77 ± 63 (26)	Absent HMW	Chronic severe TCP
V1314D (2B)	MG	3.53 ± 0.19 (3)	0.25 (1)	45 ± 50 (1)	Absent HMW	Severe TCP

[a]See the Supporting Material for literature reporting patient clinical data.
[b]N, native (native structure with varying thermodynamic stability); NL, nativelike (defined by a reduced secondary structure content with a urea and thermal unfolding transition); and MG, molten globule (defined by lack of a urea and thermal unfolding transition).
[c]NB, no binding. Pause times are reported as the mean ± SD of the number of experimental measurements made in parentheses.
[d]Clinical data reported as the mean ± SD of all reported data in the referenced literature (see Table S1 for the primary literature data). The number of reported values are in parentheses. NR, not reported. vWF:RCo/vWF:Ag ratio and platelet counts are reported for a similar G1324A substitution.
[e]HMW, high molecular weight; ATS, abnormal triplet structure.
[f]RiPB, ristocetin-induced platelet binding; BiPB, botrocetin-induced platelet binding; SPA, spontaneous platelet aggregation; TCP, thrombocytopenia. Adjectives describing TCP are quoted directly from the authors.
[g]Some clinical data also included from the analogous mutation G1324A due to insufficient clinical data on G1324S.

normal multimer analysis, although some variants can reduce HMW multimers. Type 2B can have reduced or absent HMW multimers but not in all cases, and enhanced RIPA can usually distinguish type 2B from type 2A. Consequently, the results of all these tests must be carefully and statistically compared relative to one another, making accurate diagnosis of type-2 vWD subtypes difficult.

The measurement of vWF ristocetin cofactor activity is a common diagnostic test performed in clinics worldwide, quantifying the ability of a patient's plasma to agglutinate platelets in the presence of the antibiotic, ristocetin. This diagnostic is normalized to vWF antigen, a measure of the plasma concentration of vWF. A quantitative correlation between platelet pause times and vWF:RCo/vWF:Ag ratios (Fig. 6 *B*) was not expected because of high clinical interlaboratory variance (~20–50%) (29–32). Ristocetin was quickly removed from clinical practice due to the haphazardous thrombocytopenia and blood clotting resulting from the agent (33,34). This hematologic complication initially proved useful as a research tool for the investigation of platelet aggregation (35) leading to its prevalent use in clinical diagnostic standards worldwide. However, vWF:RCo activity is the worst performing assay of its class because of its imprecision, poor limit of detection (28,36), and the fact that it was not initially designed as a functional diagnostic. Rather, it was originally intended to detect the absence of a clotting factor associated with FVIII before vWF was known to be the factor responsible for disease

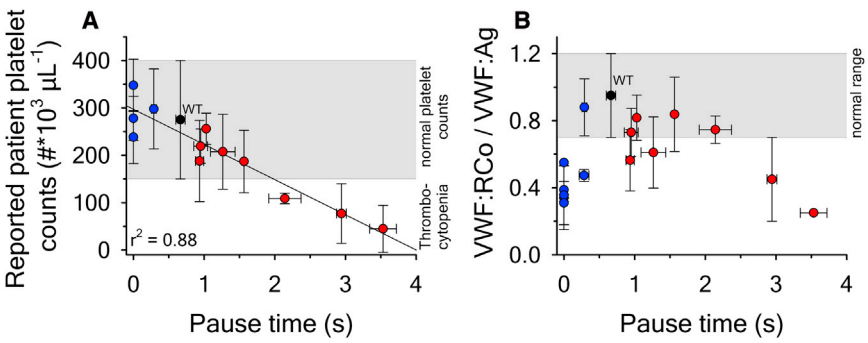

FIGURE 6 (*A*) Platelet counts reported for vWD patients with known mutations as a function of the platelet pause times obtained at 1500 s^{-1} shear rate shown in Fig. 5. The linearity has a correlation coefficient of determination ($R^2 = 0.88$). (*B*) The ratio of vWF ristocetin cofactor activity relative to vWF antigen levels reported for vWD patients. (*Gray areas*) Normal range of these clinical metrics. (*Red*) Type 2B; (*blue*) type 2M. Data points at zero pause time represent the type 2M mutations for which there was no shear-dependent binding. These data are also tabulated in Table 1 with the primary clinical data given in Table S1. To see this figure in color, go online.

(37,38). Despite some monoclonal antibody evidence for ristocetin binding to distinct sites on vWF (39,40), ristocetin's action is not specific because it binds many proteins, particularly within proline and glycine-containing β-turn regions, and flocculates many large polymeric proteins (41).

A fundamental limitation of today's functional diagnostics is that they cannot account for the conformational dynamics of the protein structures involved in the rheological binding between platelets and vWF. Recognizing these limitations, the Biorheology Scientific Subcommittee of the International Society of Thrombosis and Hemostasis (Carrboro, NC), has considered the potential use of shear-flow assays in phenotyping vWD (42,43). We have demonstrated that platelet pause times do quantitatively correlate to reported vWD patient platelet counts and the severity of thrombocytopenia (Fig. 6 *A*). This is a promising observation because it indicates that the functional and structural effects of these particular amino-acid substitutions in the single A1 domain are representative of their effects in multimeric plasma vWF (11). In addition, it illustrates that our method of flow-chamber surface chelation preserves the innate conformation of the A1 domains without complications due to nonspecific surface adsorption. The correlation also emphasizes the dynamic range of pause times attainable by these domain variants. Rather than shifting the shear rate dependencies to higher or lower tether forces as previously shown by single molecule measurements (17,18,23), these mutations specifically alter the conformation of the A1 domain in ways that pathologically alter the strength of platelet adhesion at all shear rates. The effect of raising or lowering the pause time magnitude over the full range of physiological shear necessitates a fresh perspective on the rheology and structure of the A1:GPIbα tether bond.

Following crystal structure determinations of WT A1 (44), two type 2B variants (R1306Q and I1309V) (45), and their complexes with GPIbα (46–48), many molecular dynamics simulations have been performed (23,49–52). However, the starting structures and those resulting from these simulations are representative of only local conformational changes within the native state ensemble, and the forced dissociation of the complex cannot account for misfolded conformations. Because >60% of the variants described here are not natively structured, it is clear that the A1 domain has a significant propensity to misfold. Although the global native fold is not significantly different between WT, R1306Q, and I1309V (20), it is possible that the local structural changes observed in silico could represent events that lead to a molten globule state with enhanced function. Within the natively-structured class, the gain-of-function variants R1306Q and I1309V show local changes in the α1-β2-loop (47) and the internalization of a water molecule as a wedge between this loop and the α2-helix (48), respectively.

These conformational differences are likely a result of the loss of a R1306 salt bridge to D1451 in the α6-helix and a loss of hydrophobic interactions between I1309 and P1337 at the beginning of the α2-helix. Molecular dynamics has recently shown that these mutations result in a pendulum-like movement of the α2-helix away from the domain with the largest deviation occurring at the N-terminus. These conformational changes could increase its propensity for unfolding under shear stress (53). Our structural studies show that, although the secondary structure content of these variants is unchanged, these mutations increase accessibility of the tryptophan and moderately enhance the exposed hydrophobic surface area (Fig. 3, *D* and *F*). Functionally, the effect of I1309V on platelet pause times is more severe than R1306Q, presumably because of the more direct and localized effect on the α2-helix hydrophobic packing.

The P1337L mutation occurring at the N-terminus of the α2-helix induces a molten globule state that has enhanced platelet pause times. This could be due to a loss of localized polyproline-II structure constraining the backbone- and/or hydrophobic-packing problems imposed by the leucine side chain. The reduced secondary structure content and enhanced tryptophan accessibility and hydrophobic surface area of this variant imply that the structure and stability of the α2-helix could be perturbed. Similarly, the nativelike R1341Q variant is the least thermodynamically stable and its position in the α2-helix may eliminate salt-bridge contacts with either E1305 in α1-helix or the N-terminal E1264. This could result in destabilization of the α2-helix and enhance its propensity to unfold under shear stress. In molecular dynamics, dissociation of the α2-helix was accompanied by a salt-bridge switch from R1341-E1305 to R1341-E1264 (53).

The V1314D and V1316M variants in the β2-strand have the largest pause times and are associated with the most severe thrombocytopenias observed in vWD patients. Refolding of these molten globule variants is highly improbable due to either the insertion of a negatively charged aspartate or methionine-induced steric hindrances in the hydrophobic core. Given that the valine side chains are directed toward α1- and α2-helices, these substitutions have substantial effects on the tertiary structural contacts holding this region together. Taking into account all the variants that cluster in this region, it is probable that the α2-helix is inhibitory to GPIbα binding, and destabilization or unfolding of this helix leads to an enhanced capacity to bind platelets under shear stress.

Conversely, the native R1308L variant represents an anomaly in that it is clinically assigned as a type 2B mutation despite normal bleeding times, vWF multimers, vWF:RCo/vWF:Ag ratios, and the absence of thrombocytopenia in patients (26,27,54). The only evidence for a type 2B phenotype was low RIPA and reduced collagen binding (26,55). However, in our system it clearly has reduced platelet function because platelet pause times are shorter

than those obtained with WT A1. R1308L is natively structured and induces local increases in tryptophan accessibility and hydrophobic surface area due to the removal of R1308-W1313 stacking interactions and substitution of the leucine side chain. Reduced platelet adhesiveness to this variant might be explained by the enhanced thermodynamic stability due to efficient hydrophobic packing within the α1-β2-loop region. Therefore, we reclassify R1308L as belonging to subtype 2M.

An intriguing observation is that molten globule conformations can also result in completely disabled platelet adhesive function. The I1425F and S1285F variants that occur in the α5-helix and β1-α1-loop, respectively, introduce large hydrophobic packing interferences due to the imposed phenyl side chain and globally misfold and inactivate the A1 domain. Additionally, two specific variants in this class, E1359K and F1369I, located adjacent to the binding site in the α3-helix, result in the most disordered molten globule conformations. Similar to another type 2M K1362T mutation (56), the charge reversal in E1359K may disrupt a helix stabilizing salt bridge between E1359 and K1362. Furthermore, the α3-helix, which appears to be anchored to the domain by hydrophobic interactions with F1369, is destabilized by the F1369I substitution. In the loop following the α3-helix, R1374H may disrupt a potential salt bridge to D1277 in the β1-strand. Given the location of E1359K and F1369I, the α3-helix may stabilize structural contacts that enable binding and the more distant I1425F and S1285F mutations may allosterically affect this region and/or other regions required for binding.

G1324S is the only type 2M mutation that remains natively structured, and it is the most thermodynamically stable of the variants investigated here. Interpreting how this variant causes complete loss of function, based on structure alone, remains elusive because the location is solvent-exposed. In the complex, this region directly hydrogen-bonds with the GPIbα β-hairpin. A possible mechanism is that glycine enhances conformational fluctuations and allows protein structures to sample locally unfolded states in the energy landscape without changing the ground-state structure (57). Substitution of a serine effectively reduces the ϕ-ψ conformational space, introducing rigidity into this region of structure. Rigidity is also artificially introduced here in the WT A1 domain crystal structure by chelation of divalent Cd^{2+} between H1322 and H1326, and the β-hairpin of GPIbα forces rigidity by continuing the central β-sheet in the cocrystal complex (44). Another mechanism might also be that placing a side chain containing amino acid in position 2 of a type-I β-hairpin turn is unfavorable, because glycine predominantly occurs in this position. Therefore, serine could simply destabilize the β-turn and prevent antiparallel β-strand hydrogen bonds necessary for binding to GPIbα in the native state.

The fact that both gain- and loss-of-function molten globules occur in the A1 domain supports the idea that specific structural elements are required for the A1-GPIbα interaction whereas others elements are inhibitory. Although the possibility of binding-induced refolding of the A1 to the native state from the molten globule state exists, this scenario is not probable because the forces on vWF resulting from shear stress of blood flow and tensile stress of platelet adhesion favor less-ordered conformations (58). Furthermore, a relaxed conformation of the A1 domain induced by carboxyamidation of the disulfide bond, which is incapable of refolding, results in such tight binding of GPIb to remaining secondary structure elements that platelets become arrested under shear flow (19). Inspection of the structural locations of these mutations and their effect on the functional and conformational properties of the A1 domain suggests that the α2- and α3-helices are probable secondary structure elements involved in misfolding to pathological conformations of the A1 domain. However, it is clear that mutations distant from the binding site also affect structure and function indicating that allosterism contributes in addition to more localized structural effects.

SUPPORTING MATERIAL

Mutagenesis, Expression, Purification, and Quantification of the vWF A1 Variants, two tables, seven figures, and one movie are available at http://www.biophysj.org/biophysj/supplemental/S0006-3495(14)00744-9.

We acknowledge Cellix Ltd. for the custom design of the biochips used in the flow chamber studies and Jack Aviv for the Near-UV-CD cylindrical cell holder. We also acknowledge Drs. Raul A. Urrutia, Marina Ramirez-Alvarado, Miguel A. Cruz, William L Nichols, John A. Heit, and Dong Chen for comments on the manuscript.

This work was supported by National Heart Lung and Blood Institute of the National Institutes of Health grant No. HL109109 to M.A.

REFERENCES

1. Rodeghiero, F., G. Castaman, and E. Dini. 1987. Epidemiological investigation of the prevalence of von Willebrand's disease. *Blood.* 69:454–459.
2. Lillicrap, D. 2013. von Willebrand disease: advances in pathogenetic understanding, diagnosis and therapy. *Blood.* http://dx.doi.org/10.1182/blood-2013–06–498303.
3. Peyvandi, F., T. Kunicki, and D. Lillicrap. 2013. Genetic sequence analysis of inherited bleeding diseases. *Blood.* 122:3423–3431.
4. Weiss, H. J., V. T. Turitto, and H. R. Baumgartner. 1978. Effect of shear rate on platelet interaction with subendothelium in citrated and native blood. I. Shear rate-dependent decrease of adhesion in von Willebrand's disease and the Bernard-Soulier syndrome. *J. Lab. Clin. Med.* 92:750–764.
5. Sadler, J. E., B. B. Shelton-Inloes, …, E. W. Davie. 1985. Cloning and characterization of two cDNAs coding for human von Willebrand factor. *Proc. Natl. Acad. Sci. USA.* 82:6394–6398.
6. Titani, K., S. Kumar, …, K. Fujikawa. 1986. Amino acid sequence of human von Willebrand factor. *Biochemistry.* 25:3171–3184.
7. Mancuso, D. J., E. A. Tuley, …, J. E. Sadler. 1989. Structure of the gene for human von Willebrand factor. *J. Biol. Chem.* 264:19514–19527.
8. Randi, A. M., S. Jorieux, …, J. E. Sadler. 1992. Recombinant von Willebrand factor Arg^{578}→Gln. A type IIB von Willebrand disease

mutation affects binding to glycoprotein Ib but not to collagen or heparin. *J. Biol. Chem.* 267:21187–21192.

9. Cooney, K. A., W. C. Nichols, …, D. Ginsburg. 1991. The molecular defect in type IIB von Willebrand disease. Identification of four potential missense mutations within the putative GpIb binding domain. *J. Clin. Invest.* 87:1227–1233.
10. Rabinowitz, I., E. A. Tuley, …, J. E. Sadler. 1992. von Willebrand disease type B: a missense mutation selectively abolishes ristocetin-induced von Willebrand factor binding to platelet glycoprotein Ib. *Proc. Natl. Acad. Sci. USA.* 89:9846–9849.
11. Cruz, M. A., T. G. Diacovo, …, R. I. Handin. 2000. Mapping the glycoprotein Ib-binding site in the von Willebrand factor A1 domain. *J. Biol. Chem.* 275:19098–19105.
12. Rastegar-Lari, G., N. Ajzenberg, …, D. Baruch. 2001. Defect of heparin binding in plasma and recombinant von Willebrand factor with type 2 von Willebrand disease mutations. *Thromb. Haemost.* 86:1459–1465.
13. Stepanian, A., A. S. Ribba, …, D. Meyer. 2003. A new mutation, S1285F, within the A1 loop of von Willebrand factor induces a conformational change in A1 loop with abnormal binding to platelet GPIb and botrocetin causing type 2M von Willebrand disease. *Br. J. Haematol.* 120:643–651.
14. Miyata, S., S. Goto, …, Z. M. Ruggeri. 1996. Conformational changes in the A1 domain of von Willebrand factor modulating the interaction with platelet glycoprotein Ibα. *J. Biol. Chem.* 271:9046–9053.
15. Miyata, S., and Z. M. Ruggeri. 1999. Distinct structural attributes regulating von Willebrand factor A1 domain interaction with platelet glycoprotein Ibα under flow. *J. Biol. Chem.* 274:6586–6593.
16. Auton, M., M. A. Cruz, and J. Moake. 2007. Conformational stability and domain unfolding of the von Willebrand factor A domains. *J. Mol. Biol.* 366:986–1000.
17. Auton, M., C. Zhu, and M. A. Cruz. 2010. The mechanism of vWF-mediated platelet GPIbα binding. *Biophys. J.* 99:1192–1201.
18. Auton, M., E. Sedlák, …, M. A. Cruz. 2009. Changes in thermodynamic stability of von Willebrand factor differentially affect the force-dependent binding to platelet GPIbα. *Biophys. J.* 97:618–627.
19. Tischer, A., P. Madde, …, M. Auton. 2014. A molten globule intermediate of the von Willebrand factor A1 domain firmly tethers platelets under shear flow. *Proteins.* 82:867–878.
20. Tischer, A., M. A. Cruz, and M. Auton. 2013. The linker between the D3 and A1 domains of vWF suppresses A1-GPIbα catch bonds by site-specific binding to the A1 domain. *Protein Sci.* 22:1049–1059.
21. Tischer, A., and M. Auton. 2013. Urea-temperature phase diagrams capture the thermodynamics of denatured state expansion that accompany protein unfolding. *Protein Sci.* 22:1147–1160.
22. Blancas-Mejía, L. M., A. Tischer, …, M. Ramirez-Alvarado. 2014. Kinetic control in protein folding for light chain amyloidosis and the differential effects of somatic mutations. *J. Mol. Biol.* 426:347–361.
23. Yago, T., J. Lou, …, C. Zhu. 2008. Platelet glycoprotein Ibα forms catch bonds with human WT vWF but not with type 2B von Willebrand disease vWF. *J. Clin. Invest.* 118:3195–3207.
24. Auton, M., K. E. Sowa, …, M. A. Cruz. 2010. Destabilization of the A1 domain in von Willebrand factor dissociates the A1A2A3 tri-domain and provokes spontaneous binding to glycoprotein Ibα and platelet activation under shear stress. *J. Biol. Chem.* 285:22831–22839.
25. Kim, J., C. Z. Zhang, …, T. A. Springer. 2010. A mechanically stabilized receptor-ligand flex-bond important in the vasculature. *Nature.* 466:992–995.
26. Baronciani, L., A. B. Federici, …, P. M. Mannucci. 2005. Expression studies on a novel type 2B variant of the von Willebrand factor gene (R1308L) characterized by defective collagen binding. *J. Thromb. Haemost.* 3:2689–2694.
27. Federici, A. B., P. M. Mannucci, …, P. G. De Groot. 2009. Clinical and molecular predictors of thrombocytopenia and risk of bleeding in patients with von Willebrand disease type 2B: a cohort study of 67 patients. *Blood.* 113:526–534.
28. Favaloro, E. J. 2011. Diagnosis and classification of von Willebrand disease: a review of the differential utility of various functional von Willebrand factor assays. *Blood Coagul. Fibrinolysis.* 22:553–564.
29. Hayes, T. E., J. T. Brandt, …, M. T. Cunningham. 2006. External peer review quality assurance testing in von Willebrand disease: the recent experience of the United States College of American Pathologists proficiency testing program. *Semin. Thromb. Hemost.* 32:499–504.
30. Kitchen, S., I. Jennings, …, F. E. Preston. 2006. Laboratory tests for measurement of von Willebrand factor show poor agreement among different centers: results from the United Kingdom National External Quality Assessment Scheme for Blood Coagulation. *Semin. Thromb. Hemost.* 32:492–498.
31. Meijer, P., and F. Haverkate. 2006. An external quality assessment program for von Willebrand factor laboratory analysis: an overview from the European concerted action on thrombosis and disabilities foundation. *Semin. Thromb. Hemost.* 32:485–491.
32. Nichols, W. L., M. E. Rick, …, M. Weinstein. 2009. Clinical and laboratory diagnosis of von Willebrand disease: a synopsis of the 2008 NHLBI/NIH guidelines. *Am. J. Hematol.* 84:366–370.
33. Gangarosa, E. J., N. S. Landerman, …, E. G. Herndon, Jr. 1958. Hematologic complications arising during ristocetin therapy; relation between dose and toxicity. *N. Engl. J. Med.* 259:156–161.
34. Flood, V. H., K. D. Friedman, …, R. R. Montgomery. 2009. Limitations of the ristocetin cofactor assay in measurement of von Willebrand factor function. *J. Thromb. Haemost.* 7:1832–1839.
35. Howard, M. A., and B. G. Firkin. 1971. Ristocetin—a new tool in the investigation of platelet aggregation. *Thromb. Diath. Haemorrh.* 26:362–369.
36. Chandler, W. L., E. I. B. Peerschke, …, P. Meijer. 2011. von Willebrand factor assay proficiency testing. The North American Specialized Coagulation Laboratory Association experience. *Am. J. Clin. Pathol.* 135:862–869.
37. Howard, M. A., R. J. Sawers, and B. G. Firkin. 1973. Ristocetin: a means of differentiating von Willebrand's disease into two groups. *Blood.* 41:687–690.
38. Weiss, H. J., L. W. Hoyer, …, J. Rogers. 1973. Quantitative assay of a plasma factor deficient in von Willebrand's disease that is necessary for platelet aggregation. Relationship to factor VIII procoagulant activity and antigen content. *J. Clin. Invest.* 52:2708–2716.
39. Girma, J. P., Y. Takahashi, …, D. Meyer. 1990. Ristocetin and botrocetin involve two distinct domains of von Willebrand factor for binding to platelet membrane glycoprotein Ib. *Thromb. Haemost.* 64:326–332.
40. De Luca, M., D. A. Facey, …, M. C. Berndt. 2000. Structure and function of the von Willebrand factor A1 domain: analysis with monoclonal antibodies reveals distinct binding sites involved in recognition of the platelet membrane glycoprotein Ib-IX-V complex and ristocetin-dependent activation. *Blood.* 95:164–172.
41. Scott, J. P., R. R. Montgomery, and G. S. Retzinger. 1991. Dimeric ristocetin flocculates proteins, binds to platelets, and mediates von Willebrand factor-dependent agglutination of platelets. *J. Biol. Chem.* 266:8149–8155.
42. Zwaginga, J. J., K. S. Sakariassen, …, J. W. Heemskerk. 2007. Can blood flow assays help to identify clinically relevant differences in von Willebrand factor functionality in von Willebrand disease types 1–3? *J. Thromb. Haemost.* 5:2547–2549.
43. Favaloro, E. J. 2008. Can blood flow assays help to identify clinically relevant differences in von Willebrand factor functionality in von Willebrand disease types 1–3? *J. Thromb. Haemost.* 6:545–546.
44. Emsley, J., M. Cruz, …, R. Liddington. 1998. Crystal structure of the von Willebrand factor A1 domain and implications for the binding of platelet glycoprotein Ib. *J. Biol. Chem.* 273:10396–10401.
45. Fukuda, K., T. A. Doggett, …, R. C. Liddington. 2002. Structural basis of von Willebrand factor activation by the snake toxin botrocetin. *Structure.* 10:943–950.
46. Huizinga, E. G., S. Tsuji, …, P. Gros. 2002. Structures of glycoprotein Ibα and its complex with von Willebrand factor A1 domain. *Science.* 297:1176–1179.

47. Dumas, J. J., R. Kumar, …, L. Mosyak. 2004. Crystal structure of the wild-type von Willebrand factor A1-glycoprotein Ibα complex reveals conformation differences with a complex bearing von Willebrand disease mutations. *J. Biol. Chem.* 279:23327–23334.

48. Celikel, R., Z. M. Ruggeri, and K. I. Varughese. 2000. von Willebrand factor conformation and adhesive function is modulated by an internalized water molecule. *Nat. Struct. Biol.* 7:881–884.

49. Chen, W., J. Lou, and C. Zhu. 2009. Molecular dynamics simulated unfolding of von Willebrand factor A domains by force. *Cell. Mol. Bioeng.* 2:75–86.

50. Chen, W., J. Lou, and C. Zhu. 2010. Simulated thermal unfolding of the von Willebrand factor A domains. *Cell. Mol. Bioeng.* 3:117–127.

51. Interlandi, G., and W. Thomas. 2010. The catch bond mechanism between von Willebrand factor and platelet surface receptors investigated by molecular dynamics simulations. *Proteins.* 78:2506–2522.

52. Li, J., L. Zhang, and Y. Sun. 2012. Molecular basis of the initial platelet adhesion in arterial thrombosis: molecular dynamics simulations. *J. Mol. Graph. Model.* 37:49–58.

53. Liu, G., Y. Fang, and J. Wu. 2013. A mechanism for localized dynamics-driven affinity regulation of the binding of von Willebrand factor to platelet glycoprotein Ibα. *J. Biol. Chem.* 288:26658–26667.

54. Lillicrap, D. 2009. Genotype/phenotype association in von Willebrand disease: is the glass half full or empty? *J. Thromb. Haemost.* 7 (*Suppl 1*): 65–70.

55. Bonnefoy, A., R. A. Romijn, …, M. F. Hoylaerts. 2006. von Willebrand factor A1 domain can adequately substitute for A3 domain in recruitment of flowing platelets to collagen. *J. Thromb. Haemost.* 4:2151–2161.

56. Rayes, J., A. Hommais, …, J. P. Girma. 2007. Effect of von Willebrand disease type 2B and type 2M mutations on the susceptibility of von Willebrand factor to ADAMTS-13. *J. Thromb. Haemost.* 5:321–328.

57. Schrank, T. P., D. W. Bolen, and V. J. Hilser. 2009. Rational modulation of conformational fluctuations in adenylate kinase reveals a local unfolding mechanism for allostery and functional adaptation in proteins. *Proc. Natl. Acad. Sci. USA.* 106:16984–16989.

58. Springer, T. A. 2011. Biology and physics of von Willebrand factor concatamers. *J. Thromb. Haemost.* 9 (*Suppl 1*):130–143.